ACS OMEGA

http://pubs.acs.org/journal/acsodf

Article

Development of MgO-sepoilite Nanocomposites against Phytopathogenic Fungi of Rice (*Oryzae sativa*): A Green Approach

Anjali Sidhu,* Anju Bala,* Harmandeep Singh, Radha Ahuja, and Amit Kumar

Cite This: *ACS Omega* 2020, 5, 13557−13565

Read Online

ACCESS | Metrics & More | Article Recommendations

ABSTRACT: Innovation in agriculture is a vital organ of research for sustainable food supply to the increasing global population. Organic compounds used as fungicidal agents against seed-borne pathogens are bracketed due to their toxic nature and residual effects, which are either already banned or may get banned in the near future. In this study, the surface and electric properties of nontoxic sepiolite have been blended with the antimicrobial properties of metabolizable MgO nanoforms (nMgO) as a greener alternative to prepare their nanocomposites. We compared a sepiolite-MgO (SE-MgO) nanocomposite with MgO nanoparticles in an aqua dispersed form (aqMgO-NPs) for their antifungal evaluation against various phytopathogenic fungi of rice. The SE-MgO nanocomposite was more potent in comparison to aqMgO-NPs with ED_{90} > 230 and 249 μg/mL, respectively, against the test fungi better than standard fungicides. Ultramicroscopic studies revealed hyphal distortion and spore collapse as the cause of antimycotic activity. The in vitro seed treatment revealed 100% hyphal reduction with SE-MgO at 250 μg/mL of MgO as an active ingredient (a.i.). MgO and sepiolite both have been regarded as safe materials by international agencies; therefore, using their nanocomposites can be an effective, sustainable, nontoxic, eco-friendly, and residue-free strategy for combating fungal menace against phytopathogens.

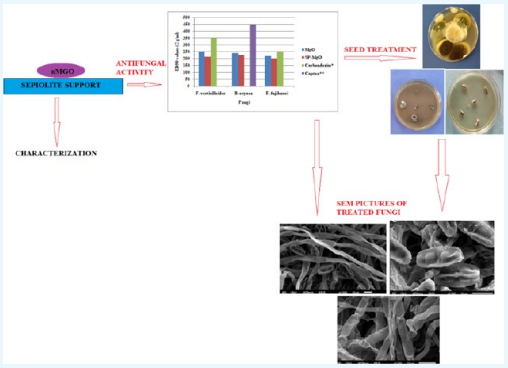

INTRODUCTION

Nanocomposites are multicomponent solid materials composed of a polymer matrix or a continuous phase with a discontinuous phase or filler. Nanocomposites are made by the incorporation of nanofillers with nanoscale lengths in at least one dimension.[1] The incorporation of known antimicrobial nanoparticles into polymeric, ceramic, or metallic matrices enables the creation of new-generation materials with improved physical and antimicrobial properties. These matrices not only provide support for the nanoparticles but can also enhance the antimicrobial performance to widen their potential applications.

Silicate-based nanocomposites (nanoclays) are interesting systems to hold a broad type of active substances with a wide range of industrial applications. Food and Agriculture Organization of the United Nations (FAO) recognizes silicates as a permitted substance for the production of organic foods in the category "Substances for plant pest and disease control". Sepiolite, a magnesium silicate ($Si_{12}O_{30}Mg_8(OH,F)_4(H_2O)_4 \cdot 8H_2O$), is a natural clay that is considered as nonhazardous and noncarcinogenic by the International Agency for Research on Cancer (IARC).[2] It provides an aperture to assemble a wide variety of organic and inorganic species[3,4] for their biomedical applications. The presence of a high density of surface silanol groups in sepiolite allows hydrogen-bonding interactions with diverse organic species.[3] The negatively charged surface ensures ionic interactions in the assembly of sepiolite with inorganic cations. The nanocomposites and bio-nanohybrid of sepiolite represent alluring prospects for biomedical applications in the fields of biosensors, scaffolds for tissue engineering, effective drug-delivery nanovehicles, vaccination, and wound dressings.[5−9]

Many nanoparticles have been identified as fillers for making polymer nanocomposites to improve their antimicrobial performances. Silver, copper, copper oxide,[10] titanium oxide, tellurium nanoparticles, carbon nanotubes (CNTs), and their two-dimensional counterpart, graphene nanoplatelets (GNPs)[11] have been well explored as nanocomposites in the biomedical field, water treatment, and food industries. Heavy-metal nanoparticles are discouraged due to their inherent toxicity risks as well as their nonmetabolizable nature and possible accumulation in the food chain. In contrast, magnesium oxide nanoparticles (nMgO) are an attractive alternative to heavy-metal-based nanoparticles because nMgO can be degraded and metabolized efficiently in the body, and the

Received: January 1, 2020
Accepted: May 25, 2020
Published: June 2, 2020

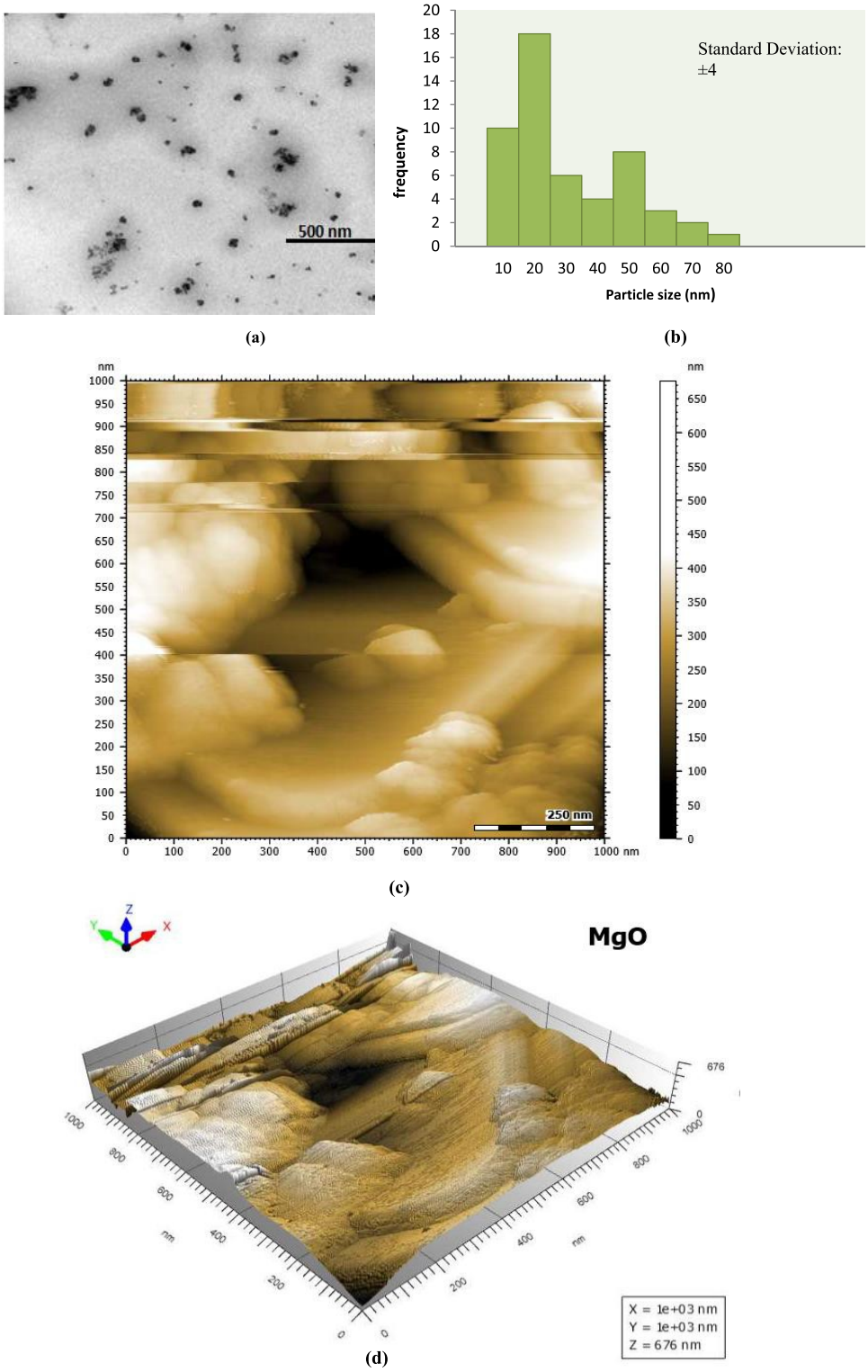

Figure 1. (a) TEM image, (b) histogram, and (c, d) AFM images of MgO-NPs: (c) two-dimensional (2D) view and (d) three-dimensional (3D) view.

released degradation products of Mg^{2+} and OH^- ions can be effectively eliminated from the body as long as the renal function is normal, thus removing the concerns of excessive metal accumulation in the body.[12] They are also recognized as safe materials by the United States Food and Drug Administration.[13] nMgO are coming up as an attractive alternative to heavy-metal-based nanoparticles in the antimicrobial regime.

MgO nanoparticles (nMgO) have become interesting for bioapplications due to their antimicrobial properties. Tang and Lv[14] have reviewed nMgO as an antibacterial agent against Gram-positive, Gram-negative, and endospore-forming bacteria.[15−20] The antibacterial properties of nMgO under different conditions are well documented and hence proven. The antifungal potency of nMgO is still in its infancy with very little literature and proven mechanistic details. Koka et al.[21] evaluated

https://dx.doi.org/10.1021/acsomega.0c00008
ACS Omega 2020, 5, 13557−13565

the antifungal activity of magnesium oxide (MgO) nanoparticles against rot-causing fungi. The antifungal activity of nMgO significantly inhibited the spores of *Alternaria alternata*, *Fusarium oxysporum*, *Rhizopus stolonifer*, and *Mucor plumbeus*.[22] nMgO and its ZnO:MgO and ZnO:$Mg(OH)_2$ nanocomposites inhibited the strains of *Colletotrichum gloeosporioides*, in turn inhibiting the germination of conidia and structural damage to the fungal cells.[23] The application of MgO- and Zn-doped MgO NPs showed important antifungal properties, inhibiting the epilithic and endolithic colonization of *Aspergillus niger* and *Penicillium oxalicum*.[24]

The previous papers on MgO nanoforms do not provide any concrete information on antifungal evaluation against phyto- or human pathogens of fungal nature.[21,22,24] To take full advantage of nMgO as antifungal agents, two different physical formulations of MgO, viz., nMgO in aqua dispersed form and its composite with sepiolite, were prepared for their in vitro screening against *Fusarium verticillioides*, *Bipolaris oryzae*, and *Fusarium fujikuroi*, the economically important fungus of rice. Their mechanistic details were explored from ultramicroscopic morphographs. In vitro seed treatment studies on infested rice seeds gave implicit visualization of the relative effects of two physically dissimilar forms of nMgO.

RESULTS AND DISCUSSION

Characterization of aqMgO-NPs. MgO-NPs in aqua dispersed form were used for transmission electron microscopy (TEM), scanning electron microscopy−energy-dispersive spectroscopy (SEM-EDS), and UV−visible analysis. X-ray diffraction (XRD) and atomic force microscopy (AFM) involved ultracentrifugation of aqueous form at 4000 rpm for 1 h to get solid pellets for analysis.

TEM images of aqMgO-NPs, synthesized using thermal treatment,[25] confirmed the nanometer size and distorted spherical morphology with aggregation (Figure 1a). The particle size range varied from 10 to 20 nm with an average size of 15 ± 4 nm (Figure 1b). Niu et al.[26] reported similar shapes of MgO NPs and size in the range of 14−32 nm, which were in agreement with those reported by Vatsha et al.[25] Two- and three-dimensional topographies of MgO nanoparticles over a 1 × 1 μm scan are shown in Figure 1c,d respectively. Tapping-mode AFM experiments were performed using commercial etched silicon tips as AFM probes. Topological images revealed distorted elliptical-shaped MgO NPs, which were similar to those obtained from SEM images (Figure 2a). The EDS analysis confirmed the elemental composition of the MgO nanoparticles containing magnesium (Mg) and oxygen (O), close to 1:1 atomic ratio with carbon as impurity. The presence of 50% of oxides and 18% magnesium confirmed the elemental composition of MgO nanoparticles (Figure 2b,c). The peak corresponding to carbon resulted from the grid.

The expected crystalline phase of nMgO was confirmed by the standard peaks in the XRD pattern. The peaks at 2θ values of 36.9, 42.9, and 62.3° in the 2θ range can be indexed to the (1 1 1), (2 0 0), and (2 2 0) planes of the face-centered cubic (FCC) structured MgO-NPs (Figure 2e).[27] The average crystallite size of MgO NPs was calculated to be 16.11 nm from full width at half-maxima (FWHM) of all peaks using the Debye−Scherrer equation, which was in agreement with the TEM results.

Maximum absorption (λ_{max}) was observed at 278 nm (Figure 2d) using a UV−visible spectrophotometer. The λ_{max} values and optical properties of MgO-NPs were in agreement with the literature.[26] The optical properties of the metal oxide NPs were

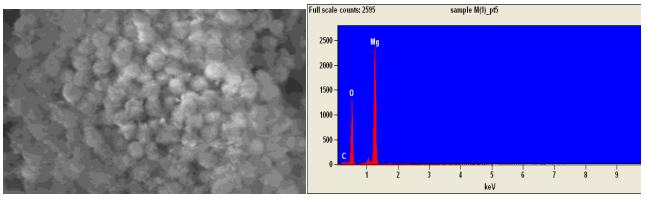

(a) (b)

Element	Weight %	Atom %
C	23.59	31.84
O	49.66	50.32
Mg	26.75	17.84
Total	100.00	100.00

(c)

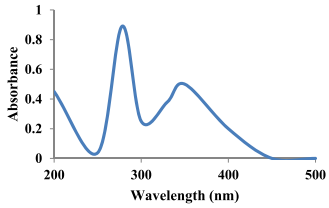

(d)

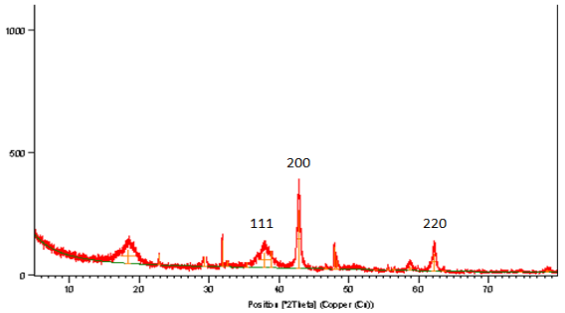

(e)

Figure 2. (a) SEM image of MgO NPs; (b, c) elemental composition of MgO-NPs; and (d) UV analysis and (e) XRD pattern of MgO-NPs.

measured in freshly prepared dispersions as well as in the same dispersions after regular intervals of 15 days for up to 4 months. There were no significant diversions from the starting values, revealing the long shelf life of the prepared nanodispersions.

Characterization of SE-MgO Nanocomposites. XRD of SE-MgO nanocomposites was performed in the solid state. TEM and SEM analyses involved the dispersion of solid in deionized water without sonication so that MgO should not get detached from sepiolite base.

The morphologies of SE-MgO were analyzed by electron microscopy. In all of the three SE-MgO-1-3, nMgO were present predominantly as isolated particles, with small populations of clumping. SEM images revealed a large number of nanoparticles on the clay surface (Figure 3a−c), which increased with the increase in the percentage of active ingredient MgO in the nanocomposites. There was no difference in the morphology, shape, and size of nMgO in any sample. The results were further supported by TEM images, which show an uneven distribution of a large number of particles with a size range of 10−100 nm covering the surface of sepiolite (Figure 4a−c).

A strong diffraction peak at 2θ = 7.42 in the XRD patterns due to the two-dimensional lattice-structured sepiolite as seen in Figure 5a was observed in SE-MgO. The XRD patterns indicate no change in the structural parameters of sepiolite with the

https://dx.doi.org/10.1021/acsomega.0c00008
ACS Omega 2020, 5, 13557−13565

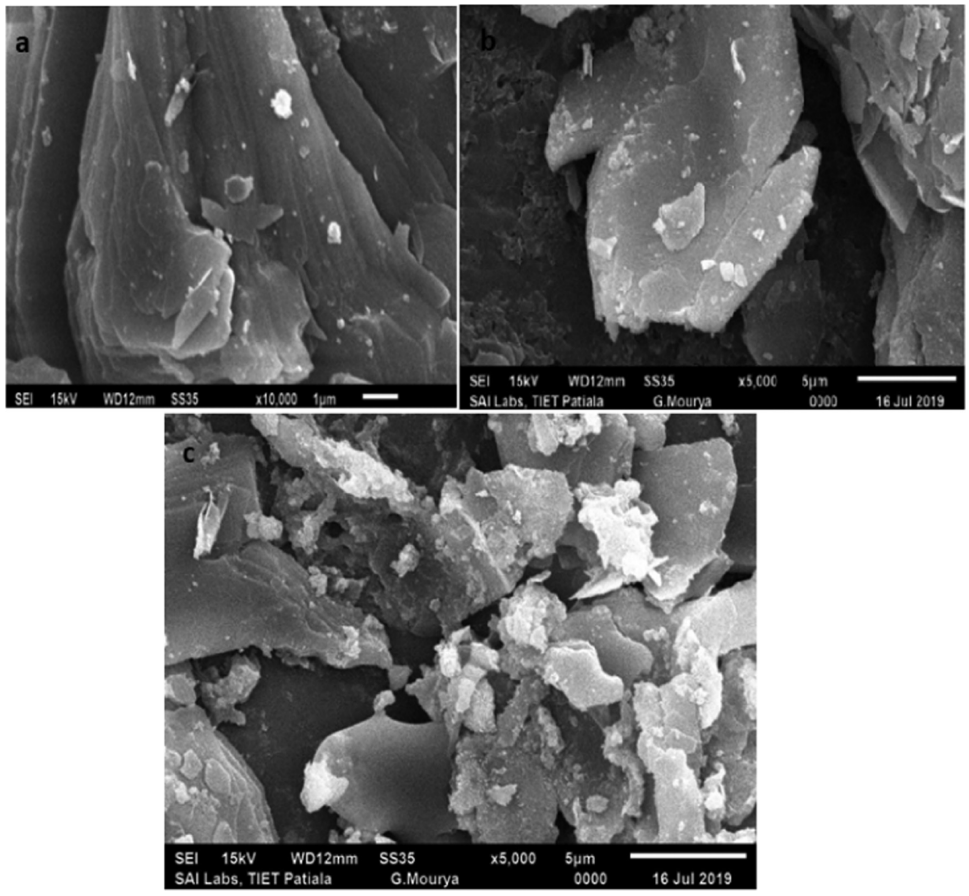

Figure 3. (a−c) SEM images of SE-MgO nanocomposites.

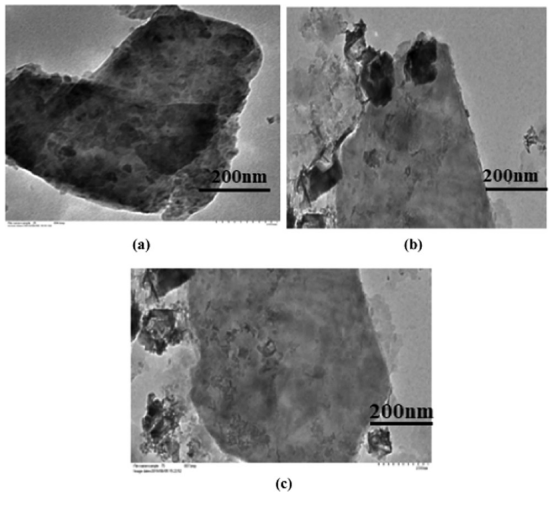

Figure 4. (a−c) TEM images of SE-MgO nanocomposites.

insertion of MgO-NPs. The XRD patterns of SE-MgO (Figure 5b−d) exhibited two families of diffraction peaks. No alteration or shifting in the peaks of sepiolite matrix was observed. In MgO, there was no base broadening of peaks indicating no variation in the particle size of MgO. The peaks of SE and MgO were revealed independently in samples SE-MgO-1-3, which confirmed the presence of two crystallites as nanocomposites formed during the in situ synthesis of SE-MgO rather than MgO-doped sepiolite.

All of the SE-MgO samples (1−3) were morphologically similar. SE-MgO-1, due to its large surface area, could provide better and even diffusion of nMgO on seed surface, and thus was selected for further antifungal evaluation studies of the three SE-MgO nanocomposites prepared.

Antifungal Evaluation Studies. The MgO nanoforms, viz., aqMgO-NPs and SE-MgO-1, were evaluated for their in vitro antifungal potential against various seed-borne phytopathogenic fungi of rice by the poisoned food technique (Figure 6a−c). The quantification of inhibition in fungal growth of *B. oryzae*, *F. verticillioides*, and *Fusarium fujikuroi*, causing seed discoloration, sheat rot, and Bakani disease in rice, respectively, demonstrated the viability of these fungi in the presence of two different formulations of nMgO.

nMgO in aqueous form inhibited the development of fungal hyphae against all three test fungi. The ED_{90} value was the lowest in the case of *F. fujikuroi* (222 μg/mL), followed by *B. oryzae* and *F. verticillioides*, with ED_{90} values of 242 and 249 μg/mL, respectively. The ED_{50} value followed the same order against all of the three test fungi for both the formulations. In the case of SE-MgO-1, the ED_{50} and ED_{90} values were ≥133 and 203 μg/mL, respectively (Table 1). SE-MgO-1 was most effective against *F. fujikuroi* with an ED_{90} value of 203 μg/mL. This pattern was the same as in aqua nMgO. The respective values against *F. verticillioides* and *B. oryzae* were 215 and 230 μg/mL. The presence of a similar order of effectiveness against all of the test fungi demonstrates the concentration dependence of fungitoxicity on nMgO.

In vitro seed treatment was done by nanopriming of infested seeds in aqMgO-NPs for 8 h and by solid application with SE-

https://dx.doi.org/10.1021/acsomega.0c00008
ACS Omega 2020, 5, 13557−13565

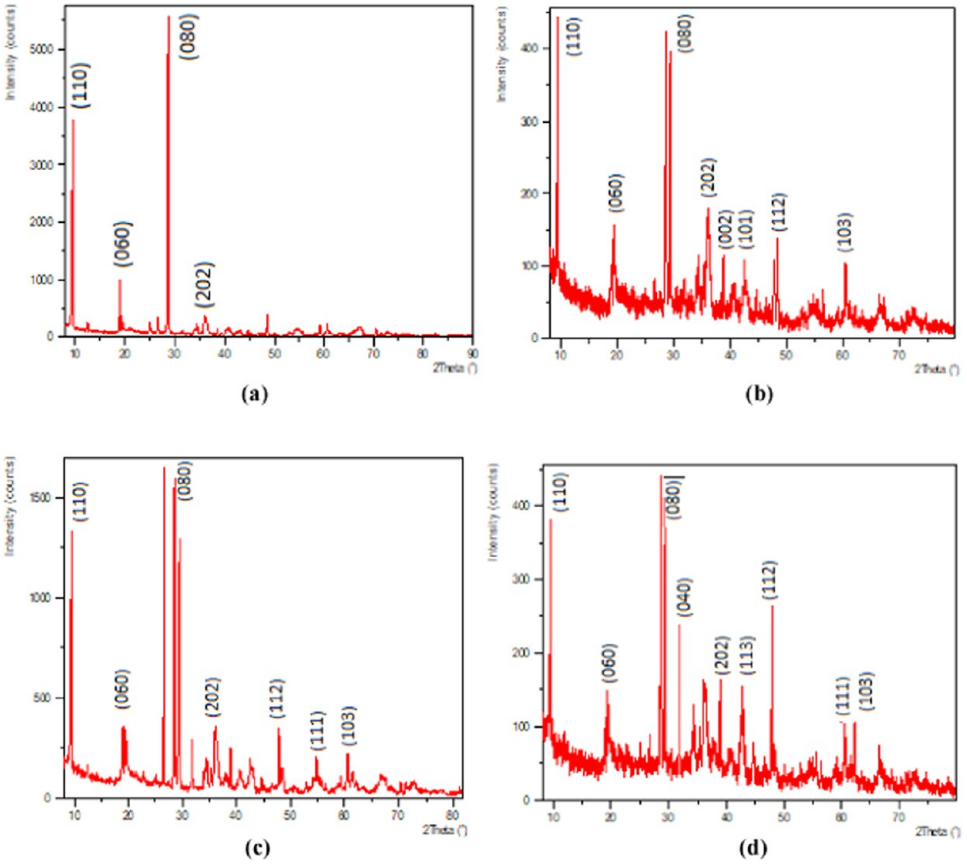

Figure 5. XRD patterns of (a) sepiolite, (b) SE-MgO-1, (c) SE-MgO-2, and (d) SE-MgO-3.

MgO-1 using 250 μg/mL of active ingredient of nMgO (a.i.) in both the cases. The treated seeds were placed on a neutral potato dextrose agar (PDA) in a Petri plate, which indicated that 250 μg/mL SE-MgO was adequate for 100% inhibition of fungal growth (Figure 7a−c). In the case of nanoprimed seeds, the fungal inhibition was <100%, inflicting the higher effectiveness of SE-MgO in the inhibition of hyphal growth than water disperse MgO nanoparticles.

The MgO-NPs aqua dispersed form exhibited higher ED_{50} and ED_{90} values in comparison to SE-MgO-1, inflicting the better potential of the prepared nanocomposites. The combination of nMgO with sepiolite formed exhibited an enhanced effect as copper sepiolite nanocomposite, as reported by Esteban-Cubillo et al.[28] against *Staphylococcus aureus* and *Escherichia coli*. The enhanced biocidal activity of nanoparticles was due to its support on the inert matrix. The activity of nMgO in aqMgO-NPs is low, and on comparing the lowest ED_{90} values of SP-MgO-1 (203 μg/mL) and aq nMgO (222 μg/mL) against *F. fujikuroi*, it was found that the antifungal activity of aq nMgO was approximately 92% (=203/222 × 100) of activity of SE-MgO. Comparative evaluation indicated that effective concentrations of aqMgO-NPs and SE-MgO-1 against *B. oryzae* were almost half that of Captan (commercial fungicide). Against *F. verticillioides* and *F. fujikuroi*, these values were again lower than those of the standard, carbendazim (ED_{50} and ED_{90} values ≥ 150 and 250 μg/mL, respectively). Nguyen et al.[29] reported nMgO to be effective against resistant strains of yeast, *Candida albicans* and *Candida glabrata* with MIC_{90} > 1.2 mg/mL (equivalent to 1200 μg/mL), a concentration much higher than that reported in our work. Monzavi et al.[30] reported a fungicidal activity of 10 mg/L nMgO with a size range of 70−150 nm against oral *C. albicans*. These values are subject to variation in size of nanoparticles, type of formulation, and experimental technique. There is a huge knowledge gap on the inhibitory effects nMgO against various fungi of phyto/human pathogenicity.

In vitro seed treatment also showed the higher activity of SE-MgO-1 than aqMgO-NPs. The native charge on the inert matrix plays a vital role in manipulation. This is analogous to the functionalization of nanoparticles with negatively charged ligands to promote their adsorption or conjugation onto the target surface. The negatively charged matrix of sepiolite in the present case can interact well with the positively charged hyphal cell wall,[31] resulting in the better interaction nature of the composite formed with fungal hyphae. Particles in aqua form can move around, spend less effective contact time on fungi for their interaction, and thus are less effective for their bioaction. There is no literature on seed treatment with nMgO for review or comparative evaluation of the antifungal character.

The visualization of the deleterious effects caused by aqMgO-NPs and SE-MgO-1 on test fungi was achieved using the SEM technique. The MgO nanoparticles caused the spores and hyphae of *B. oryzae* to shrink with visible distortions (Figure 8a,b). The hyphae appeared as ribbon shaped in comparison to the cylindrical shape in the case of control (Figure 8 c,d). There were prominent morphological alterations in the macroconidia in the case of *F fujikuroi*. The conidia got shrunken and seemed to lose their viability (Figure 9). The overall shirking of the structures may be due to pore formation in the cellular structures leading to loss of electrolyte. These results are in consonance with other nanostructures, which, owing to low size scales, caused pore formation, leading to the loss of electrolytes[32] and

https://dx.doi.org/10.1021/acsomega.0c00008
ACS Omega 2020, 5, 13557−13565

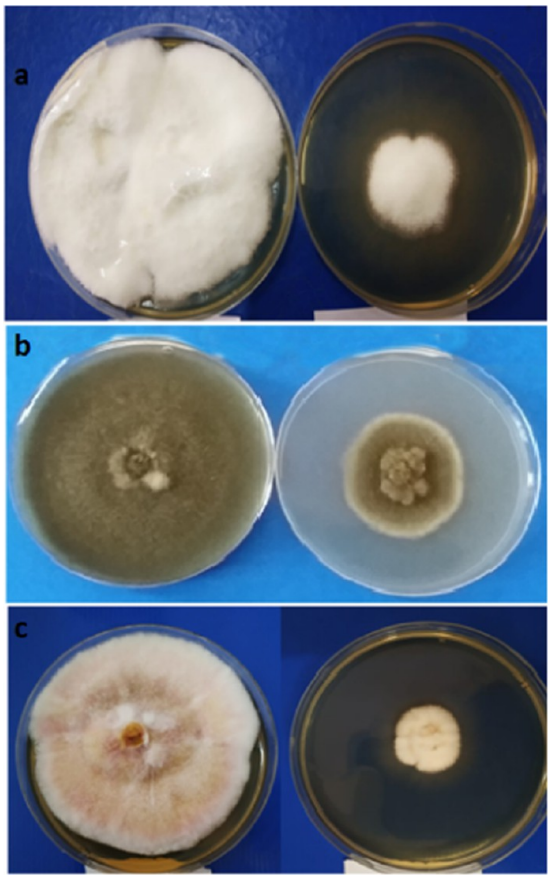

Figure 6. Antifungal activity of SE-MgO at 250 μg/mL against (a) *Fusarium verticilliodes*, (b) *B. oryzae*, and (c) *Fusarium fujikuroi* (left: control; right: test).

hence hyphal inhibition and ultimately death. A similar pattern was obtained in all of the three test fungi (Figure 10) on treatment with both MgO nanoforms, viz., aqMgO-NPs and SE-MgO-1.

The commercial fungicides carbendazim and captan are recommended at 2000 μg/mL and 3 g/kg of seeds, respectively, which are too high. Organic fungicides have a problem of pesticidal residue that remain in soil and keep on affecting the plant and animal health in the long run. The harmful effects of carbendazim on human health have been recorded in the past years due to which it is now banned in India on basmati and other crops.[33] To fulfill the great demand of eco-friendly fungicides in agriculture, scientists are in search of alternative chemicals. Pesticides of nonresidual and nontoxic nature are welcome in the next generation of pesticides. Also, single pesticide of eco-acceptable nature against multiple glitches is mandatory for the discovery of a novel molecule. nMgO qualify this mandate owing to their mycotoxic effect against all of the test fungi. Moreover, nMgO degrade and get metabolized to release Mg^{2+} and OH^- ions as degradation products via normal renal system[29] and are safe materials by international agencies. Such single solutions to multiple problems can help in unburdening the pesticidal load on food crops, after relevant studies and commercialization.

CONCLUSIONS

MgO nanoparticles are superior to other metal/metal oxide nanoparticles because of their easy degradation, metabolizable nature, and nonresidual assimilative nature. Its nanocomposite with nontoxic sepiolite, i.e., SE-MgO nanocomposite, acted as an excellent material for synergizing the antifungal potential of nMgO against all of the three seed-borne fungi of rice, viz., *F. verticillioides*, *B. oryzae*, and *F. fujikuroi*. Our study demonstrated the interactions of nMgO with fungal cell wall/membrane for the first time causing hyphal and spore disruptions, which could be the key mechanism for the disastrous effects of nMgO against the test fungi. Further research is still needed to determine the exact mechanisms for the fungicidal effects of nMgO to take full advantage of nMgO for a wide range of applications.

EXPERIMENTAL SECTION

Materials and Methods. The reagents and chemicals used were of AR grade. Magnesium nitrate, sodium hydroxide, poly(vinyl pyrollidone) (PVP), and sepiolite were purchased from Sigma-Aldrich and used with no further purification.

Characterization Techniques. The UV−visible absorption spectra of synthesized nanoparticles were recorded on a double-beam spectrophotometer (UV-1800, Shimadzu). The measurement of optical properties was carried out utilizing a quartz cell in the range of 200−800 nm. The typical morphology and diameter of nanoparticles were determined using a transmission electron microscope (Hitachi Hi-7650) by putting a drop of sample solution onto a 200-mesh carbon-covered copper grid at an accelerated voltage of 200 kV. Scanning electron micrographs of the prepared samples were recorded using an SEM model Hitachi S-3400, and SEM-EDS images of the samples were recorded on the Thermo Noran System SIX at Electron Microscopy & Nanoscience Laboratory (EMN), Punjab Agricultural University, Ludhiana. The morphologies of the prepared samples of nanoparticles were analyzed using a *Tosca* 400 Atomic Force Microscope in Application Lab, Anton Paar, Gurgaon, India. The phase compositions of all samples and nanocomposites were determined by X-ray diffraction. XRD patterns were obtained from oriented powder samples in a 2θ range of 2−80° at a scanning rate of 2°/min.

Synthesis of aqMgO-NPs. NaOH (0.4 M) was added dropwise into 0.2 M $Mg(NO_3)_2$ under constant stirring for 1 h at 60 °C. After cooling the reaction mixture to room temperature, it was centrifuged and washed with water followed by ethanol to remove impurities. The final product was dried at 80 °C for 24 h

Table 1. ED_{50} and ED_{90} values (μg/mL) of MgO-NPs and SE-MgO-1 Nanocomposites[c]

	F. verticillioides		*B. oryzae*		*F. fujikuroi*	
sample	ED_{50}	ED_{90}	ED_{50}	ED_{90}	ED_{50}	ED_{90}
MgO	180 ± 5	249 ± 2	172 ± 3	242 ± 2	145 ± 7	222 ± 8
SP-MgO-1	133 ± 2	215 ± 5	152 ± 2	230 ± 6	122 ± 8	203 ± 10
carbendazim[a]	230 ± 13	350 ± 7			150 ± 2	250 ± 6
captan[b]			275 ± 8	450 ± 10		

[a]Standard against *F. verticillioides* and *F. fujikuroi*. [b]Standard against *B. oryzae*. [c]The values are mean of triplicate values ± standard deviation.

https://dx.doi.org/10.1021/acsomega.0c00008
ACS Omega 2020, 5, 13557−13565

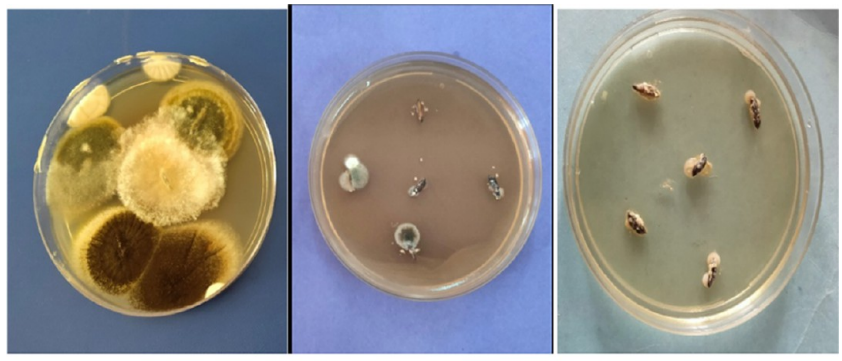

Figure 7. (a) Control having hydroprimed seeds; (b) seeds treated with MgO-NPs aqua emulsion at 250 μg/mL; and (c) seeds treated with MgO-SE at 250 μg/mL with respect to nMgO as a.i.

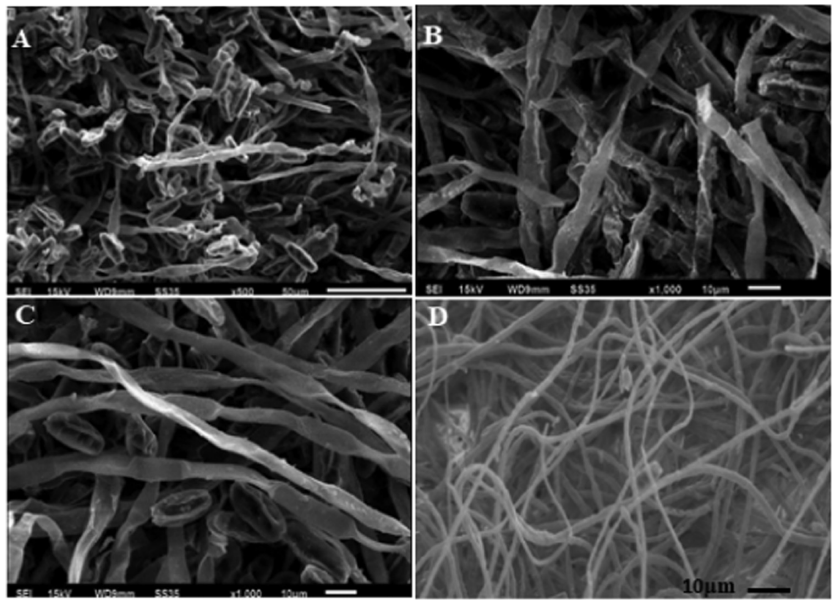

Figure 8. Scanning electron microscopy images of (A−C) treated *B. oryzae* and (D) control.

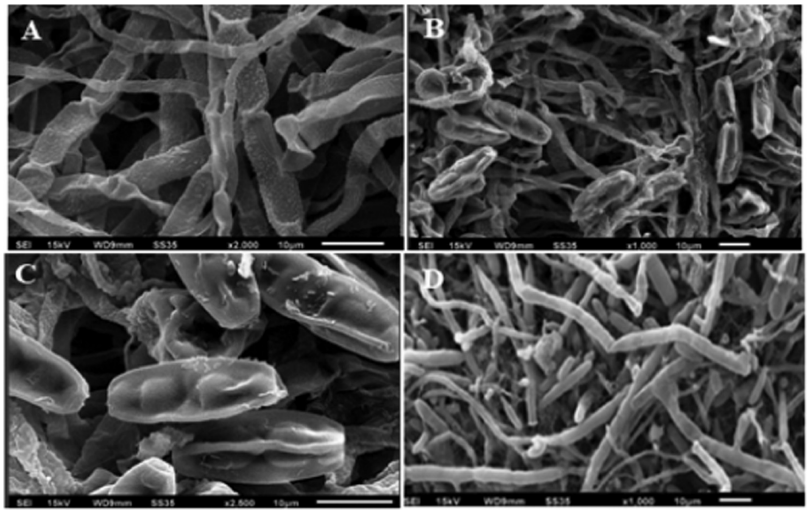

Figure 9. Scanning electron microscopy images of (A−C) treated *F. fujikuroi* and (D) control.

and then calcined at 500 °C. For bioactivity studies, 25 mg of MgO was dispersed in 50 mL of water containing Triton-X as a surfactant under sonication, which was continued for 30 min followed by PVP (as a stabilizing agent) to get stable aqMgO-NPs (500 μg/mL), and stored as a stock solution for further dilution as and when required.

https://dx.doi.org/10.1021/acsomega.0c00008
ACS Omega 2020, 5, 13557−13565

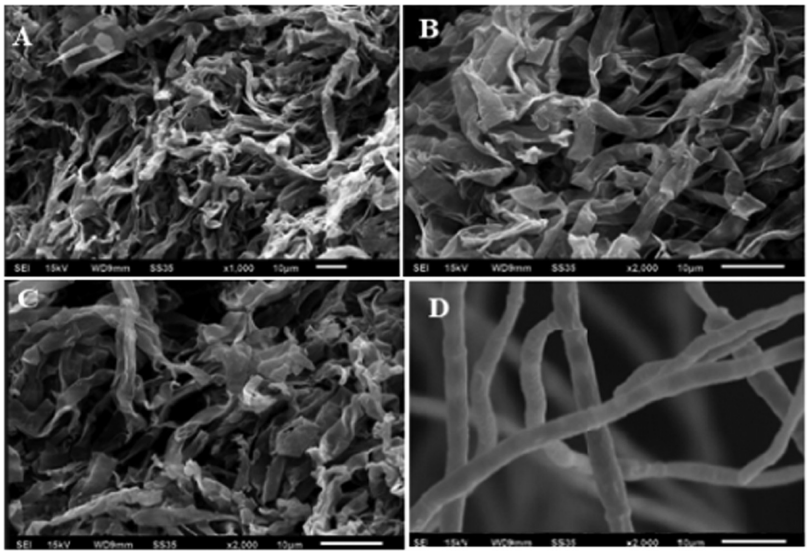

Figure 10. Scanning electron microscopy images of (A−C) treated *F. verticillioides* and (D) control.

Activation of Sepiolite. Sepiolite was activated using a well-known method.[34] One gram of sepiolite in 10 mL of 5 N HCl was stirred for 48 h. Activated sepioloite was centrifuged, washed with distilled water several times, and dried at 40 °C for 5 h in an oven.

In Situ Preparation of SE-MgO Nanocomposites. Three samples of SE-MgO nanocomposites (SE-MgO-1-3), containing 250, 500, and 750 μg/g MgO-NPs, respectively, as active ingredients were prepared.

SE-MgO-1 was prepared by suspending 10 g of activated sepiolite into a minimum quantity of deonized water in a beaker. Magnesium chloride (5.4 g) dissolved in minimum quantity of water was added to it and placed in an orbital shaker for about an hour. To the stirring solution, 2.27 g of sodium hydroxide was added and the stirring was continued for another 2 h. The contents were centrifuged and excess water was decanted off. The solid settled was collected and dried at 80 °C for 24 h and subjected to calcination at 600 °C to get the MgO-sepiolite nanocomposite-1 (SE-MgO-1) having an a.i. of MgO to be 250%.

SE-MgO-2 and SE-MgO-3 having a.i. values of MgO to be 500 and 750 μg/g, respectively, were prepared by following a similar methodology. SE-MgO-2 was prepared using 10.8 g of magnesium chloride and 4.54 g of sodium hydroxide, while SE-MgO-3 was prepared using 16.2 g of magnesium chloride and 6.81 g of sodium hydroxide.

Antifungal Potential. The antifungal activity of MgO and SE-MgO was tested against *F. verticillioides*, *B. oryzae*, and *F. fujikuroi* by the poisoned food technique at various concentrations.

SEM Analysis. Fungal culture was fixed by a well-known method[35] using a multistep protocol. The specimen was fixed in 2.5% cacodylate buffered glutaraldehyde at 4 °C for 24 h and washed thrice with a 0.1 M cacodylate buffer at 4 °C. Secondary fixation was done using 1% osmium tetraoxide at 4 °C for 2 h. Three washings were done again with a 0.1 M cacodylate buffer, each time at 4 °C. Dehydration of the sample was done by incubation with 30, 50, and 70% ethanol, each for 15 min at 4 °C, followed by dehydration with 80, 90, and 100% at room temperature. After decanting off the ethanol, the sample was placed in a vacuum desiccator overnight. The dried sample was placed on conductive carbon tabs on an aluminum stub. The samples were imaged by a Hitachi S-3400N SEM at 15 kV.

In Vitro Seed Treatment Studies. MgO-NPs in aqua dispersed form were used as a priming agent for infested seeds. The infested seeds (10 g) were dipped in 10 mL of 250 μg/mL aqMgO-NPs, resulting in an effective concentration of 250 μg of MgO-NPs per milligram of the seeds. Optimum water was added for complete dipping of seeds. After 8 h,[36] the seeds were placed aseptically on Petri plates containing solidified PDA medium. The Petri plates were incubated at 25 ± 1 °C and were observed for 6 days, with a regular interval of 24 h. The hydroprimed infested seeds were used as control for relative evaluation studies.

SE-MgO-1 (10 g) was applied uniformly on 10 g of infested rice seeds to afford 250 μg of nMgO per gram of seed. The minimum amount of water was added for proper sticking of composite on the seed surface. The seeds were placed on Petri plates, incubated, and observed in a manner similar to aqMgO-NPs application.

Statistical Analysis. The percentage inhibition data were subjected to Probit analysis to determine ED_{50} values using IBM SPSS 23 software.[37]

AUTHOR INFORMATION

Corresponding Authors

Anjali Sidhu − *Department of Chemistry, Punjab Agricultural University, Ludhiana 141004, India;* orcid.org/0000-0003-0013-9558; Email: anjalisidhu@pau.edu

Anju Bala − *Department of Plant Breeding and Genetics, Punjab Agricultural University, Ludhiana 141004, India;* Email: anjusharma@pau.edu

Authors

Harmandeep Singh − *Department of Chemistry, Punjab Agricultural University, Ludhiana 141004, India*

Radha Ahuja − *Department of Chemistry, Punjab Agricultural University, Ludhiana 141004, India*

Amit Kumar − *Department of Chemistry, Punjab Agricultural University, Ludhiana 141004, India*

Complete contact information is available at: https://pubs.acs.org/10.1021/acsomega.0c00008

https://dx.doi.org/10.1021/acsomega.0c00008
ACS Omega 2020, 5, 13557−13565

Notes

The authors declare no competing financial interest.

■ ACKNOWLEDGMENTS

The authors gratefully thank NanoMission, DST, New Delhi, India (SR/NM/NAT-02/2015), for providing financial support.

■ REFERENCES

(1) Matthews, F. L.; Rawlings, R. D. *Composite Materials: Engineering and Science*; Elsevier, 1999.
(2) Wilbourn, J. D.; McGregor, D. B.; Partensky, C.; Rice, J. M. IARC reevaluates silica and related substances. *Environ. Health Perspect.* **1997**, *105*, 756−758.
(3) Ruiz-Hitzky, E. Molecular access to intra crystalline tunnels ofsepiolite. *J. Mater. Chem.* **2001**, *11*, 86−91.
(4) Singer, A.; Galan, E. *Developments in Palygorskite-sepiolite Research: A New Outlook on these Nanomaterials*; Elsevier, 2011.
(5) Wicklein, B.; Darder, M.; Aranda, P.; Ruiz-Hitzky, E. Phospholipid−Sepiolite Biomimetic Interfaces for the Immobilization of Enzymes. *ACS Appl. Mater. Interfaces* **2011**, *3*, 4339−4348.
(6) Ruiz-Hitzky, E.; Darder, M.; Aranda, P.; delBurgo, M. ÁM.; del Real, G. Bionanocomposites as New Carriers for Influenza Vaccines. *Adv. Mater.* **2009**, *21*, 4167−4171.
(7) Ruiz-Hitzky, E.; Darder, M.; Aranda, P.; Ariga, K. Advances in biomimetic and nanostructured biohybrid materials. *Adv. Mater.* **2010**, *22*, 323−336.
(8) Yu, W. H.; Li, N.; Tong, D. S.; Zhou, C. H.; Lin, C. X.; Xu, C. Y. Adsorption of proteins and nucleic acids on clay minerals and their interactions: A review. *Appl. Clay Sci.* **2013**, *80*−*81*, 443−452.
(9) Wicklein, B.; Darder, M.; Aranda, P.; Ruiz-Hitzky, E. Bio-organoclays Based on Phospholipids as Immobilization Hosts for Biological Species. *Langmuir* **2010**, *26*, 5217−5225.
(10) Duncan, T. V. Applications of nanotechnology in food packaging and food safety: Barrier materials, antimicrobials and sensors. *J. Colloid Interface Sci.* **2011**, *363*, 1−24.
(11) Matharu, R. K.; Ciric, L.; Edirisinghe, M. Nanocomposites: Suitable Alternatives as Antimicrobial Agents. *Nanotechnology* **2018**, *29*, No. 282001.
(12) Nguyen, N.-Y. T.; Grelling, N.; Wetteland, C. L.; Rosario, R.; Liu, H. Antimicrobial Activities and Mechanisms of Magnesium Oxide Nanoparticles (nMgO) against Pathogenic Bacteria, Yeasts, and Biofilms. *Sci. Rep.* **2018**, *8*, No. 16260.
(13) https://www.accessdata.fda.gov/scripts/cdrh/cfdocs/cfcfr/CFRSearch.cfm?fr=184.1431.
(14) Tang, Z. X.; Lv, B. F. MgO Nanoparticles As Antibacterial Agent: Preparation And Activity. *Braz. J. Chem. Eng.* **2014**, *31*, 591−601.
(15) Wetteland, C. L.; Nguyen, N. Y.; Tand Liu, H. Concentration-dependent behaviors of bone marrow derived mesenchymal stem cells and infectious bacteria toward magnesium oxide nanoparticles. *Acta Biomater.* **2016**, *35*, 341−356.
(16) Krishnamoorthy, K.; Manivannan, G.; Kim, S. J.; Jeyasubramanian, K.; Premanathan, M. Antibacterial activity of MgO nanoparticles based on lipid peroxidation by oxygen vacancy. *J. Nanopart. Res.* **2012**, *14*, No. 1063.
(17) Stoimenov, P. K.; Klinger, R. L.; Marchin, G. L.; Klabunde, K. J. Metal oxide nanoparticles as bactericidal agents. *Langmuir* **2002**, *18*, 6679−6686.
(18) Jin, T.; He, Y. Antibacterial activities of magnesium oxide (MgO) nanoparticles against foodborne pathogens. *J. Nanopart. Res.* **2011**, *13*, 6877−6885.
(19) Sawai, J.; Kojima, H.; Igarashi, H.; Hashimoto, A.; Shoji, S.; Sawaki, T.; Hakoda, A.; Kawada, E.; Kokugan, T.; Shimizu, M. Antibacterial characteristics of magnesium oxide powder. *World J. Microbiol. Biotechnol.* **2000**, *16*, 187−194.
(20) Cai, L.; Chen, J.; Liu, Z.; Wang, H.; Yang, H.; Wei, D. Magnesium Oxide Nanoparticles: Effective Agricultural Antibacterial Agent Against Ralstonia solanacearum. *Front. Microbiol* **2018**, *9*, No. 790.
(21) Koka, J. A.; Wani, A. H.; Bhat, M. Y. Evaluation of antifungal activity of Magnesium oxide (MgO) and Iron oxide (FeO) nanoparticles on rot causing fungi. *J. Drug Delivery Ther.* **2019**, *9*, 173−178.
(22) Wani, A. H.; Shah, M. A. A unique and profound effect of MgO and ZnO nanoparticles on some plant pathogenic fungi. *J. Appl. Pharm. Sci.* **2019**, *2*, 40−44.
(23) De la Rosa-García, S. C.; Martínez-Torres, P.; Gómez-Cornelio, S.; Corral-Aguado, M. A.; Quintana, P.; Gómez-Ortíz, N. M. Antifungal Activity of ZnO and MgONanomaterials and Their Mixtures against *Colletotrichum gloeosporioides* Strains from Tropical Fruit. *J. Nanomater.* **2018**, *2018*, No. 3498527.
(24) Sierra-Fernandez, A.; De la Rosa-García, S. C.; Gomez-Villalba, L. S.; Gómez-Cornelio, S.; Rabanal, M. E.; Fort, R.; Quintana, P. Synthesis, Photocatalytic, and Antifungal Properties of MgO, ZnO and Zn/Mg Oxide Nanoparticles for the Protection of Calcareous Stone Heritage. *ACS Appl. Mater. Interfaces* **2017**, *9*, 24873−24886.
(25) Vatsha, B.; Teyana, P.; Shumbula, P. M.; Ngila, J. C.; Sikhwivhilu, L. M.; Moutoali, R. M. Effects of precipitation temperature on nanoparticle surface area and antibacterial behavior of Mg(OH)2 and MgO nanoparticles. *J. Biomater. Nanobiotechnol.* **2013**, *4*, 365−373.
(26) Niu, K. Y.; Yang, J.; Sun, J.; Du, X. \ One-step synthesis of MgO hollow nanospheres with blue emission. *Nanotechnology* **2013**, *21*, No. 295604.
(27) Singh, N.; Singh, P. K.; Shukla, A.; Singh, S.; Tandon, P. Synthesis and Characterization of Nanostructured Magnesium Oxide: Insight from Solid-State Density Functional Theory Calculations. *J. Inorg. Organomet. Polym.* **2016**, *26*, 1413−1420.
(28) Esteban-Cubillo, A.; Pecharromán, C.; Aguilar, E.; Santarén, J.; Moya, J. S. Antibacterial activity of copper monodispersed nanoparticlesinto sepiolite. *J. Mater. Sci.* **2006**, *41*, 5208−5212.
(29) Nguyen, N. T.; Nathaniel, G.; Cheyann, L. W.; Romeo, Rosario.; Huinan, L. Antimicrobial activities and mechanisms of magnesium oxide nanoparticles (nMgO) against pathogenic bacteria, Yeasts, and Biofilms. *Sci. Rep.* **2018**, *8*, No. 16260.
(30) Monzavi, A.; Eshraghi, S.; Hashemian, R.; Momen-Heravi, F. *In vitro* and *ex vivo* antimicrobial efficacy of nano-MgO in the elimination of endodontic pathogens. *Clin. Oral Invest.* **2015**, *19*, 349−356.
(31) Lyden, A.; Lombardi, L.; Sire, W.; Li, P.; Simpson, J. C.; Butler, G.; Lee, G. U. Characterization of carboxylate nanoparticle adhesion with the fungal pathogen *Candida albicans*. *Nanoscale* **2017**, *9*, 15911−15922.
(32) Nasrollahi, A.; Pourshamsian, K.; Mansourkiaee, P. Antifungal activity of silver nanoparticles on some of fungi. *Int. J. Nano Dimens.* **2011**, *1*, 233−239.
(33) https://www.tribuneindia.com/news/punjab/state-bans-nine-pesticides/807340.html.
(34) Kalaiselvi, C. M.; Sivakumar, R.; Subadevi, A. Activation of sepiolite by various acid treatments. *Int. Res. J. Eng. Technol.* **2017**, *4*, 19−22.
(35) Bozzola, J. J.; Russell, L. D. *Electron Microscopy: Principles and Techniques for Biologists*; Jones and Bartlett Publishers: Boston, 1999; pp 670−671.
(36) Sidhu, A.; Barmota, H.; Bala, A. Antifungal evaluation studies of copper sulfide aqua-nanoparticles and its impact on seed quality of rice (*Oryzae sativa*). *Appl. Nanotechnol.* **2017**, *7*, 681−689.
(37) Finney, D. J. *Probit Analysis*; Cambridge University Press: Cambridge, 1971.

https://dx.doi.org/10.1021/acsomega.0c00008
ACS Omega 2020, 5, 13557−13565